Engineering Structures 259 (2022) 114206

Contents lists available at ScienceDirect

Engineering Structures

journal homepage: www.elsevier.com/locate/engstruct

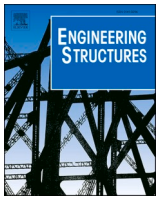

Experimental analysis on circular concrete-filled steel tubular beam-columns under unequal load eccentricities

V. Albero [a,*], C. Ibañez [b], D. Hernández-Figueirido [a], A. Piquer [a]

[a] Department of Mechanical Engineering and Construction, Universitat Jaume I, Castellón, Spain
[b] Concrete Science and Technology Institute, Universitat Politècnica de València, Valencia, Spain

ARTICLE INFO

Keywords:
Steel–concrete composite beam-columns
Unequal load eccentricity
Concrete-filled steel tubular columns
Equivalent moment factor
Experimental testing

ABSTRACT

This paper presents eight experimental tests on circular concrete-filled steel tubular (CFST) beam-columns loaded under unequal eccentricities at both ends. This loading scheme has not been widely studied yet in previous research works on CFST columns, but it may be very common into industrial or residential multi-storey frames, where both ends are subjected to different bending moments. Tests results revealed that the ultimate resisting load increases when the column is loaded under unequal eccentricities compared to what is loaded under equal eccentricities. However, under certain conditions, the column ductility decreases. Also, the equations provided by the Eurocode 4 and AISC 360–16 for second order effects were assessed. Specifically, the equivalent moment factors, βor C_m, were calculated from experimental data and compared to those given by the standards. Although Eurocode 4 presents more accurate predictions, both codes provide safe predictions for higher slenderness beam-columns but unsafe predictions for double curvature members with low slenderness. In view of the results, further research is needed to improve the equivalent moment factor proposals including additional parameters apart from the loading eccentricity ratio.

1. Introduction

Circular concrete-filled steel tubular (CFST) columns have been extensively used along decades because they present constructional and structural benefits. Specifically, this composite column typology does not need reinforcement and formwork. This allows a rapid structural erection. Besides, the confinement produced by the steel tube improves the ductility of the normal or high-strength concrete infill and decreases the occurrence of local buckling in the steel tube, which is likely to occur with very low thickness, since it can only buckle outwards. The behaviour of CFST columns has been well described and summarized by *Zhao et al.* [1] and *Han et al.* [2]. Additionally, many experimental works on this column typology were compiled by *Goode and Lam* [3] and *Leon et al.* [4] providing an extensive database for further research.

Despite the large body of research about CFST columns noted above, it was found that most of them are focused on short and axial compression members and not enough experiments are available in case of slender beam-columns under unequal load eccentricities, which produces non-constant bending moment along the column length. Besides, it should be noted that this load situation is not uncommon and, for example, may appear on multi-storey frames, where columns are subjected to different bending moments at both ends. Moreover, in case of unequal eccentricities, one positive and the other negative, the beam-column presents double curvature which may importantly affect the second order effects on the element.

Regarding the analysis of circular CFST beam-columns under double curvature bending, *Kilpatrick and Rangan* [5] presented the results of an experimental program including this effect. The results showed a significant improvement of the column stiffness due to the double curvature but with loss of ductility. In turn, also *Zeghiche and Chaoui* [6] exposed results from four circular CFST beam-columns with double curvature bending and compared them with Eurocode 4 (EN 1994–1-1 [7]) provisions. The conclusion was very disturbing because Eurocode 4 [7] showed unsafe predictions for these cases.

It seems that the increase on the stiffness and strength under unequal eccentricities may come from the larger part of concrete that remains under compression when bending is lower. Moreover, due to the brittle behaviour of concrete, when column reaches the maximum capacity, the failure is achieved reducing the ductility of the system.

Apart from circular beam-columns, *Wang* [8] provided experimental results from four rectangular CFST beam-columns under double curvature bending, including two specimens tested under biaxial bending. The tests results showed higher stiffness for specimens loaded with unequal

* Corresponding author.
E-mail address: valbero@uji.es (V. Albero).

https://doi.org/10.1016/j.engstruct.2022.114206
Received 13 January 2022; Received in revised form 9 March 2022; Accepted 27 March 2022
Available online 3 April 2022

Nomenclature

A_s	Steel cross-section area
A_g	Gross cross-section area
C_m	Equivalent moment factor (AISC 360–16)
D	Column cross-section diameter
DI	Ductility index
e^{bottom}	Load eccentricity at bottom end
e^{top}	Load eccentricity at top end
f_c, f_c'	Characteristic cylinder strength of concrete
f_y	Steel yield strength
I_c	Second moment of area of the concrete part
I_a, I_s	Second moment of area of the steel part
L	Column length
L/D	Length-diameter ratio
M_{tot}	Bending moment including first and second order effects
n	Load level
N_{exp}	Maximum experimental load
$N_{pl,Rd}$	Cross-section plastic resistance
r	Eccentricity ratio ($r = e^{bottom} / e^{top}$)
t	Tube thickness

LIST OF GREEK SYMBOLS

β	Equivalent moment factor (Eurocode 4)
$\delta_{85\%}$	Axial shortening at 85 % of maximum load in the descending branch
δ_{Nmax}	Axial shortening at maximum experimental load
Δ	Lateral deflection
Δ_{Nmax}	Maximum lateral deflection along column length at maximum axial load
ε	Longitudinal strain
χ	Cross-section curvature

Table 1
Specimen details.

ID	D (mm)	t (mm)	e^{top} (mm)	e^{bottom} (mm)	r	f_y (MPa)	f_c (MPa)	$N_{pl,Rd}$ (kN)	L/D
CFST1	219.1	3	50	50	1.0	452.00	40.43	2362.6	13.69
CFST2				25	0.5	452.00	45.96	2559.8	
CFST3				0	0.0	452.00	45.96	2559.8	
CFST4				−25	−0.5	452.00	46.74	2587.6	
CFST5	108	2	50	50	1.0	387.40	40.43	601.5	27.78
CFST6				25	0.5	414.67	45.96	666.6	
CFST7				0	0.0	500.76	46.74	730.6	
CFST8				−25	−0.5	438.45	46.74	689.1	

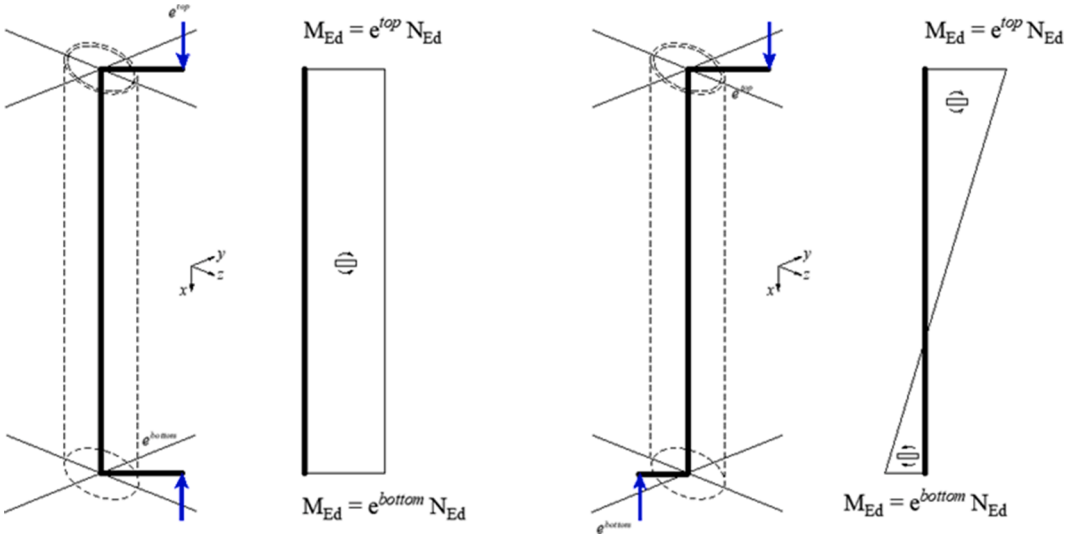

Fig. 1. Load eccentricity at ends (First order bending moment variation).

eccentricities and safe previsions were provided by BS 5400 Part 5 [9] and the current Eurocode 4 [7] for this beam-column typology. Additionally, *Hernández-Figueirido et al.* [10,11] developed an extensive experimental program on square and rectangular CFST beam-columns under unequal load eccentricities, including 36 specimens. The experiments covered eccentricity ratios from 1 to −0.5 and columns infilled with normal and high strength concrete. The tests results confirmed higher stiffness and ultimate load for beam-columns under unequal load eccentricity, but similar ductile behaviour between them was found. Moreover, the concrete strength was revealed as the most influential parameter to increase the ultimate axial load. Provisions from standards Eurocode 4 [7] and AISC 360 [12] were assessed showing slightly unsafe predictions mainly related with second order effects. Therefore, corrections on flexural stiffness ($E{\cdot}I$) and on the equivalent moment factor (β or C_m) were encouraged.

In turn, as it is referred in bibliography, the circular CFST column cross-section is the most effective geometry due to the constant confinement that the steel tube provides to the concrete core. Therefore, when the beam-column is subjected to unequal eccentricities and the part along the column under compression is larger than in beam-

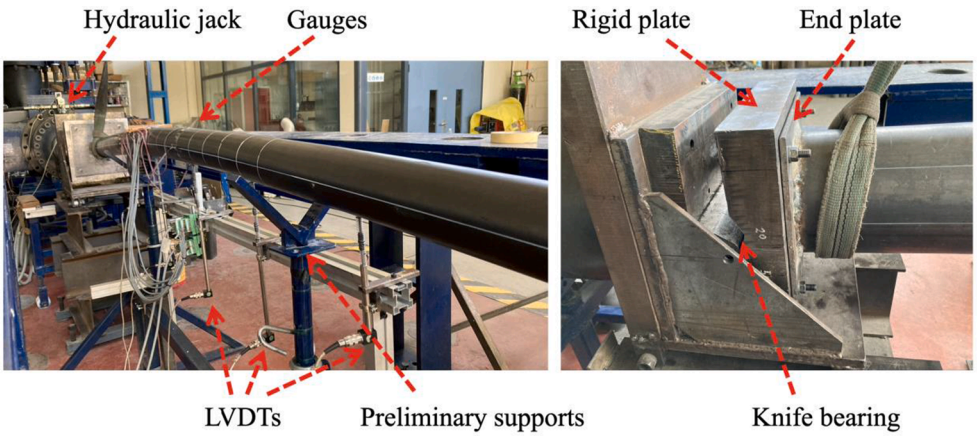

Fig. 2. Test setup view.

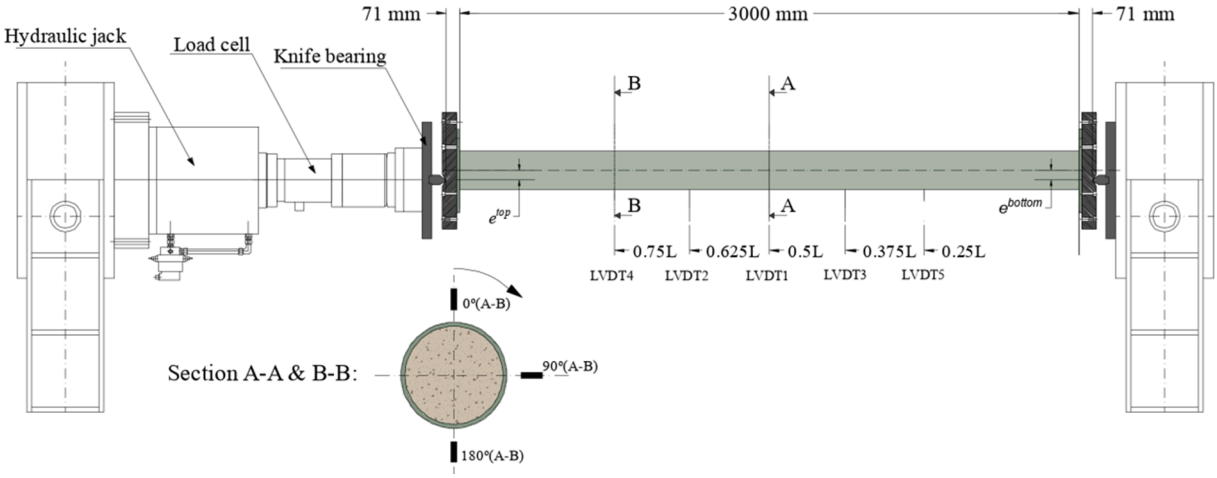

Fig. 3. Schematic view of column and devices position.

columns subjected to equal eccentricities, the column capacity seems higher for circular than for rectangular cross-sections. Additionally, related to concrete confinement, it is worthy to notice here that the size effect has been also considered in bibliography when CFST columns are applied to large-scale engineering structures under low eccentricity [13,14].

More recently, *Espinós et al.* [15] developed a finite element numerical model validated with the experiments noted previously [8] and carried out a parametric study on rectangular CFST beam-columns including the non-constant bending – i.e unequal load eccentricities at both ends- as an important factor on the ultimate load and stiffness of the columns. Other advanced models for CFST are also available for the analysis of these slender beam-columns [16].

Following the findings described above, the objective of this paper is to extend the number of experiments available regarding circular CFST beam-columns under unequal load eccentricities in order to provide a deeper understanding of this situation on the beam-column response. Besides, these experiments may contribute to build a wider database of tests which could be useful for the assessment of the accuracy of current code provisions on composite steel–concrete beam-columns. It should be noted that the experimental tests conducted in this research differ from those available in the literature due to the higher load eccentricity (up to 50 mm) and the study of intermediate eccentricity ratios from 1 to −0.5. Previous tests were limited to low eccentricities (20, 30 mm) and extreme eccentricity ratios between 1.0 and −1.0.

2. Experimental program

2.1. Specimens description

The experimental program described in this paper consists of eight circular CFST columns with a length of 3 m, divided into two groups of four specimens, see Table 1. The columns of the first group (CFST1 to CFST4) show the same geometry with 219.1 mm of steel tube diameter and 3 mm of tube thickness, which represents a 13.69 length-diameter ratio (L/D). In turn, the specimens belonging to the second group (CFST5 to CFST8) present 108 mm of tube diameter, 2 mm of tube thickness and a length-diameter ratio of 27.78. In both groups, the lowest tube thickness employed produces a diameter-thickness ratio (D/t) over the maximum value provided by EN 1994–1-1 [7] Clause 6.7.1 (9). Therefore, the thin-walled section condition should be assumed for all columns.

In turn, the difference between the specimens of each group comes from the load eccentricity at both ends. While the top eccentricity (e^{top}) equals 50 mm for all columns, the bottom eccentricity (e^{bottom}) can take the next allowable values: 50, 25, 0 and −25 mm. Therefore, the load eccentricity ratio between both ends presents values from 1 to −0.5. This variation in the loading scheme produces unequal load eccentricities at the ends and non-constant first order bending moment along the column length, see Fig. 1. Moreover, the test setup was designed to create pinned–pinned boundary conditions so the buckling length could be considered 3135 mm for all columns, including the end plate thickness. It should be highlighted that due to the column geometry (circular), the

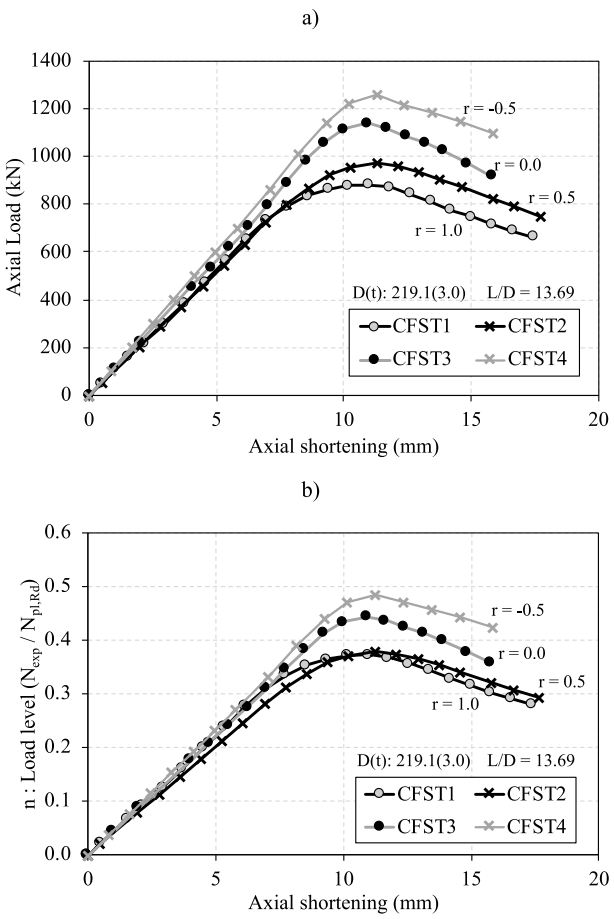

Fig. 4. CFST1-CFST4 Test results. a) Load vs. axial shortening; b) Load level vs. axial shortening.

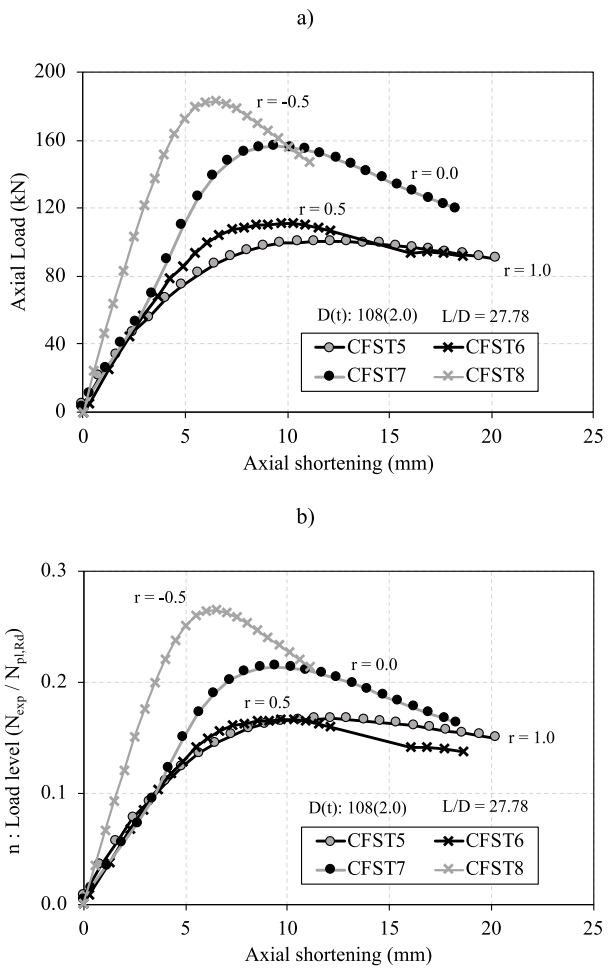

Fig. 5. CFST5-CFST8 Test results. a) Load vs. axial shortening; b) Load level vs. axial shortening.

bending analysis can be done in-plane.

About materials, it should be noted that the steel tubes were cold formed and were supplied by a manufacturer with a S275JR steel grade. However, the real steel strength (f_y) was obtained by the corresponding coupon tests for each specimen, see Table 1. It can be observed that all the specimens of the first group present the same real steel strength (452.00 MPa) because these four steel tubes came from the same manufacturing batch. However, the steel tubes of the second group were supplied from different manufacturing batches and showed a variable real steel strength from 387.40 MPa to 500.76 MPa.

Regarding the specimen preparation process, a 300x300x10 mm steel plate (S275JR) was firstly welded to the bottom end of each empty steel tube to simplify the casting of concrete and to create the joint with the pinned support assembly. Secondly, the steel tubes were cast in vertical position with normal strength fresh concrete, supplied by a local concrete producer. Finally, the column was covered by welding another steel plate to the top end. The concrete was made using calcareous aggregates with a nominal concrete strength of C30/37 MPa. The real concrete compressive strength (f_c) was determined from 150x300 mm cylinders using the standard compressive test procedure. All columns were tested further than 28 days from their casting day. Thus, the same day as each column test day, the concrete compression was measured, see Table 1.

2.2. Test setup

The specimens described previously were tested at the Universitat Jaume I, Castellon (Spain) testing facilities. A horizontal hydraulic jack with 5000 kN of maximum capacity was used. In order to apply the load under equal or unequal eccentricities at both ends a special assembly was built. Specifically, the end plates described in the previous section were welded to the steel tube with the required eccentricity which permitted applying unequal eccentric loads, but maintaining the column in horizontal position. Additionally, the end plates were screwed to a rigid plate (71 mm thick), which presents a knife form to allow for load transfer without any rotational restraint, see Fig. 2. Thus, the specimens are tested under pinned–pinned boundary conditions.

The tests were conducted under a displacement-controlled scheme, with a constant displacement velocity of 1 mm/min. This loading scheme permits the post-peak analysis. Indeed, the test was extended after the peak until the load showed at least a 15 % reduction. In order to initialise the tests from a neutral position and to avoid the self-weight effect, two vertical supports were positioned below the specimens (Fig. 2). These supports have no effect after the preload application (5.0 kN) because the eccentricity direction was placed downwards and then the columns showed always upwards displacements.

About the measurement control system, apart from the loading registration, five Linear Variable Displacement Transducers (LVDTs) were placed at five points along the column length in order to measure the column deflection during the test, see Fig. 3. Additionally, six strain gauges were located, three in the central cross-section (A) and three in one quarter intermediate cross-section (B), which registered longitudinal strains at three locations: 0°, 90° and 180° (Fig. 3).

Table 2
Test and analysis results.

ID	N_{exp} (kN)	n	δ_{Nmax} (mm)	$\delta_{85\%}$ (mm)	DI	Δ_{Nmax} (mm)	β_{exp} (EC4)	$C_{m,exp}$ (AISC 360–16)
CFST1	880.78	0.373	11.06	14.88	1.35	26.6	1.000	1.059
CFST2	968.47	0.378	11.27	15.80	1.40	24.3	0.944	1.001
CFST3	1138.81	0.445	10.93	14.85	1.36	17.5	0.788	0.836
CFST4	1256.33	0.486	11.28	16.00	1.42	14.0	0.698	0.738
CFST5	100.44	0.167	11.32	23.14	2.05	49.2	1.096	1.018
CFST6	112.85	0.169	11.03	17.57	1.59	40.9	0.916	0.842
CFST7	156.40	0.214	9.41	15.44	1.64	38.5	0.626	0.46
CFST8	183.16	0.266	6.51	10.06	1.54	28.8	0.392	0.211

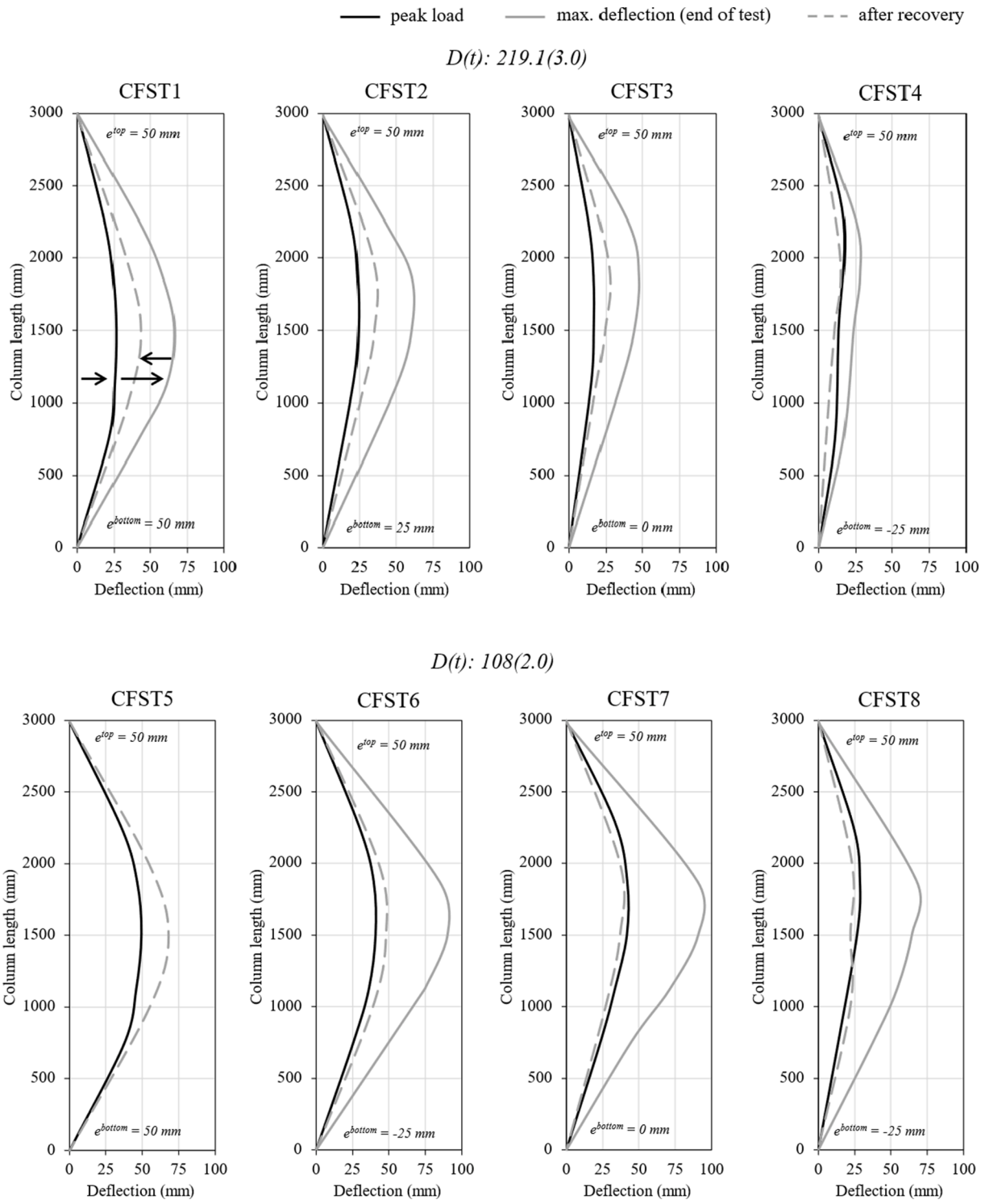

Fig. 6. Measured deflection along column length.

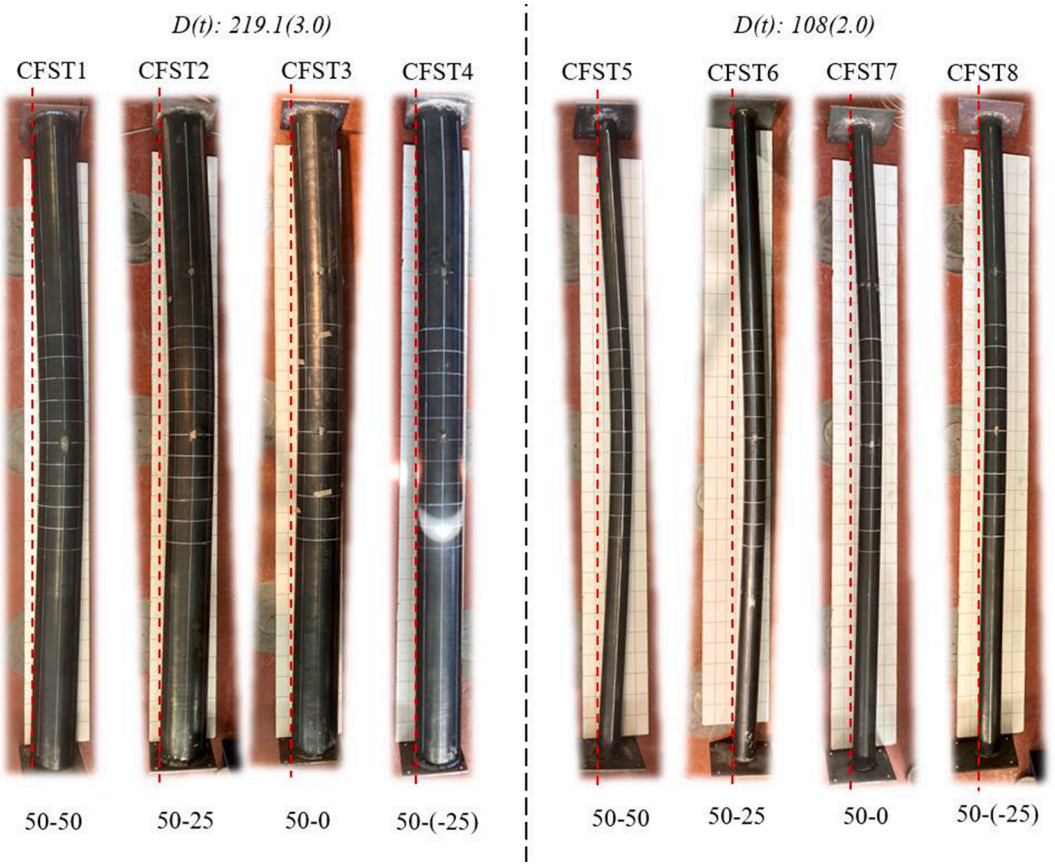

Fig. 7. Column remaining deflection after test.

3. Test results

The clearest test results, in terms of axial load versus axial shortening, are showed in Fig. 4a (CFST1 to CFST4) and Fig. 5a (CFST5 to CFST8). These two plots clearly present the increase in the maximum load when the eccentricity ratio (r) decreases from 1.0 to −0.5. Exact values of the maximum load achieved for each experiment (N_{exp}) and the axial shortening observed at this load (δ_{Nmax}) are showed in Table 2.

Although the increase in the maximum load for lower eccentricity ratios may seem obvious, it is interesting to notice the difference between Fig. 4a and Fig. 5a. While Fig. 4a for CFST1 to CFST4 columns shows similar stiffness (loading slope) and ductility (unloading slope) for all specimens, Fig. 5a for CFST5 to CFST8 shows an increase in the stiffness and a decrease in the ductility when the loading eccentricity ratio decreases (compare $r = 1.0$ and $r = -0.5$ in Fig. 5a). This behaviour, observed in Fig. 5a, matches with previous findings done by *Kilpatrick and Rangan* [5].

Apart from the direct observation of loading curves, the ductility of each column can be quantified from the ductility index (DI). DI is measured following *Han et al.* [17] proposal, as the ratio between the axial displacement corresponding to 85% of the maximum load in the descending branch ($\delta_{85\%}$) and the displacement from the maximum load (δ_{Nmax}):

$$DI = \frac{\delta_{85\%}}{\delta_{Nmax}} \tag{1}$$

The calculated DI, detailed in Table 2, shows a similar value, between 1.35 and 1.42, for columns CFST1 to CFST4. However, for specimens CFST5 to CFST8 the DI drops from 2.05 for $r = 1.0$ to 1.54 for $r = -0.5$, which confirms the lower ductility for members subjected to unequal eccentricities, as it was described before.

Additionally, it should be highlighted that the different behaviour observed between Fig. 4a and Fig. 5a may be attributed to the length-diameter ratio (L/D), which is the main parameter that changes between both figures. However, the plain plots observed in Fig. 4a and Fig. 5a should not be compared directly because the concrete compressive strength and steel yield strength are not the same for all specimens, as it was described in Table 1. In order to solve this fact, the experimental load is normalized by using the cross-section plastic resistance ($N_{pl,Rd}$). Then, the applied load can be plotted in comparable values of load level (n) on Fig. 4b and Fig. 5b, where:

$$n = \frac{N_{exp}}{N_{pl,Rd}}$$

The overall behaviour observed in Fig. 4b and Fig. 5b presents the same trend as noted for Fig. 4a and Fig. 5a. Therefore, the higher stiffness and lower ductility observed here and in previous investigations for CFST beam-columns under double curvature ($r < 0.0$) is corroborated just for specimens with high length-diameter ratio (L/D). This finding seems reasonable because these specimens also present higher second order effects. The exact values for the maximum load level during each experiment are listed in Table 2.

In turn, the deflection along the column length was measured during each test by the LVDTs described in Fig. 3. In particular, Fig. 6 displays the deflection results for each test at the peak load (black line), at the end of the test (grey line) and after the unloading (grey dashed line), which shows the unrecovered deflection due to plastic strains.

CFST1 and CFST5, with equal loading eccentricities at both ends ($r = 1.0$), show maximum deflection at the column mid-length. However, the more the loading eccentricity difference between both ends, the more the displacement of the maximum deflection point from mid-length to the top end. See the difference from CFST2 to CFST4 and from CFST6 to CFST8. Additionally, it can be observed that the deflection values of higher slenderness columns (CFST5 to CFST8) are higher than those

a) Section A-A (L/2)

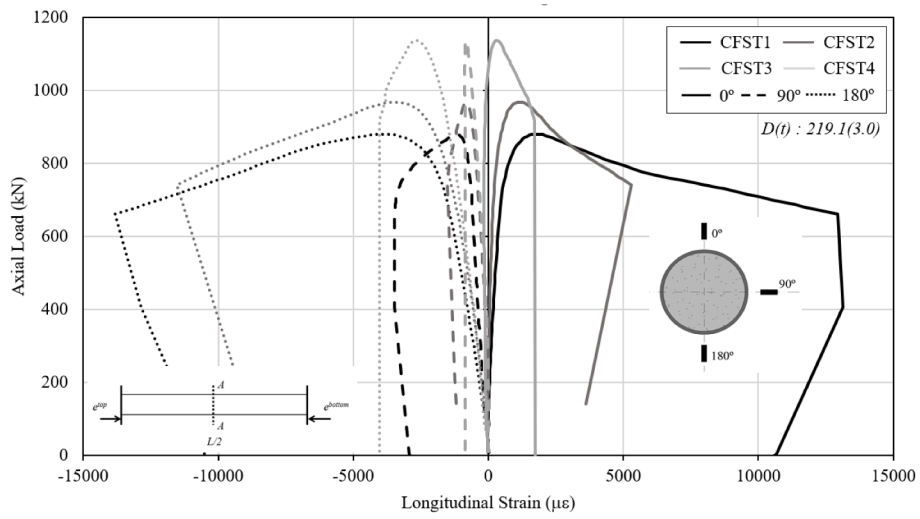

b) Section B-B (L/4)

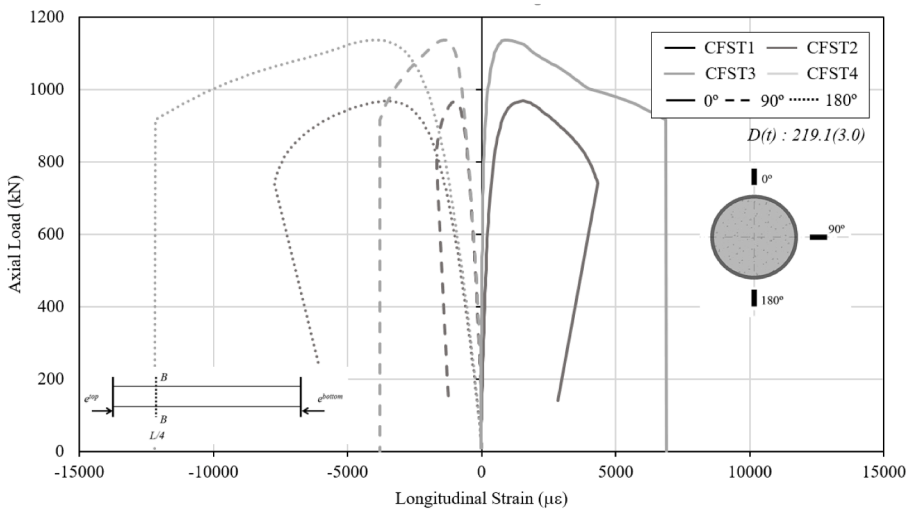

Fig. 8. Axial load versus longitudinal strain (ε_L) for specimens CFST1 to CFST4.

from CFST1 to CFST4. It should be noted here that CFST5 deflection at the end of test is not displayed in Fig. 6 because maximum elongation of LVDTs was reached. Moreover, Fig. 7 presents the real pictures of each column after the test to show the remaining deflection. A red dashed line has been included in Fig. 7 to mark the original column longitudinal axis.

Finally, the longitudinal strain gauges results are displayed in Fig. 8 for specimens CFST1 to CFST4, and in Fig. 9 for CFST5 to CFST8. Both figures show the strain measurements for the mid-length section (A-A) and the quarter-length section (B-B). In all cases, the top strain gauge (0°) shows positive values, which means tension, while lateral (90°) and bottom (180°) gauges present negative values, which are related to compression stress. These results, in terms of tension and compression, mean that the neutral line is located over the cross-sectional centre of mass. This displacement of the neutral line out of the centre of mass indicates that beam-columns are loaded under combined bending and compression. This finding from strain gauges results fits perfectly with the loading scheme, where loading eccentricity is placed below the cross-section centre of mass, and the column deflects upwards.

Additionally, longitudinal strain measurement at top ($\varepsilon_{0°}$) and bottom ($\varepsilon_{180°}$) cross-section points allows for the curvature (χ) calculation:

$$\chi = \frac{(\varepsilon_{0^o} - \varepsilon_{180^o})}{D} \tag{3}$$

This curvature can be plotted against the applied bending moment, including the second order effects, to obtain the experimental M- χ curve:

$$M = N_{exp} \cdot e^{top} + N_{exp} \cdot \Delta_{LVDT1} \tag{4}$$

The experimental moment–curvature plot (M- χ) for the mid-length cross-section of each column showed in Fig. 10 can be useful for further numerical model validation. It should be noted that the M- χ curve for CFST4 was omitted due to strain measurement errors during CFST4 test.

4. Equivalent moment factor

The experiments detailed before differ from each other only in the unequal loading eccentricities at both ends. This fact affects mainly the second order response because, as was described in Fig. 6, the column deflection changes from single to double curvature.

European and American structural standards deal with this non-

a) Section A-A (L/2)

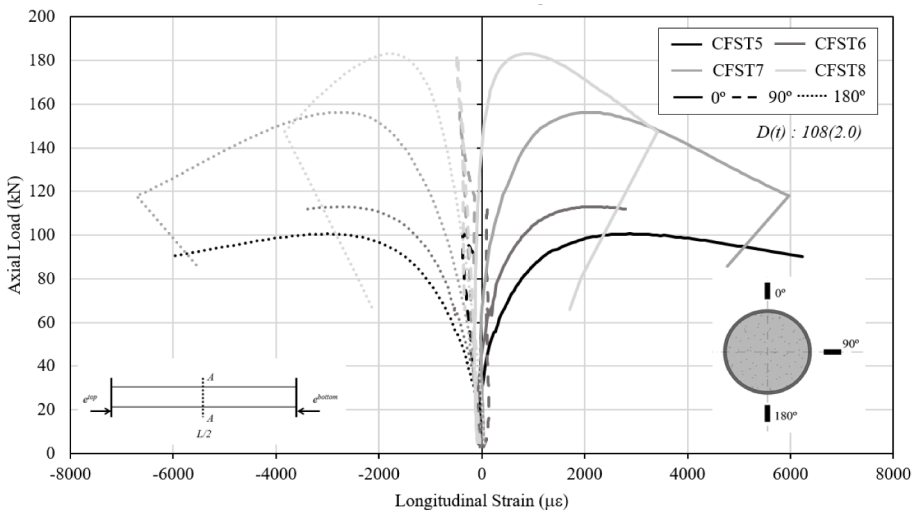

b) Section B-B (L/4)

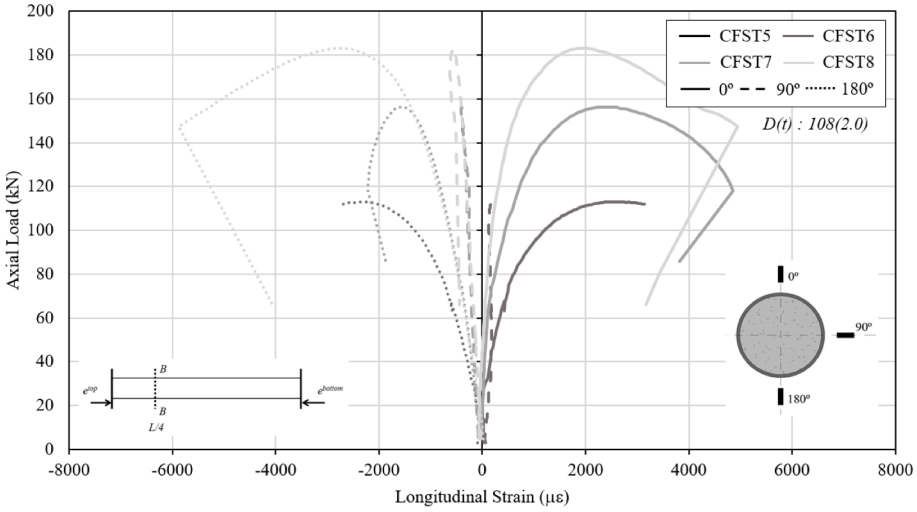

Fig. 9. Axial load versus longitudinal strain (ε_L) for specimens CFST5 to CFST8. a).

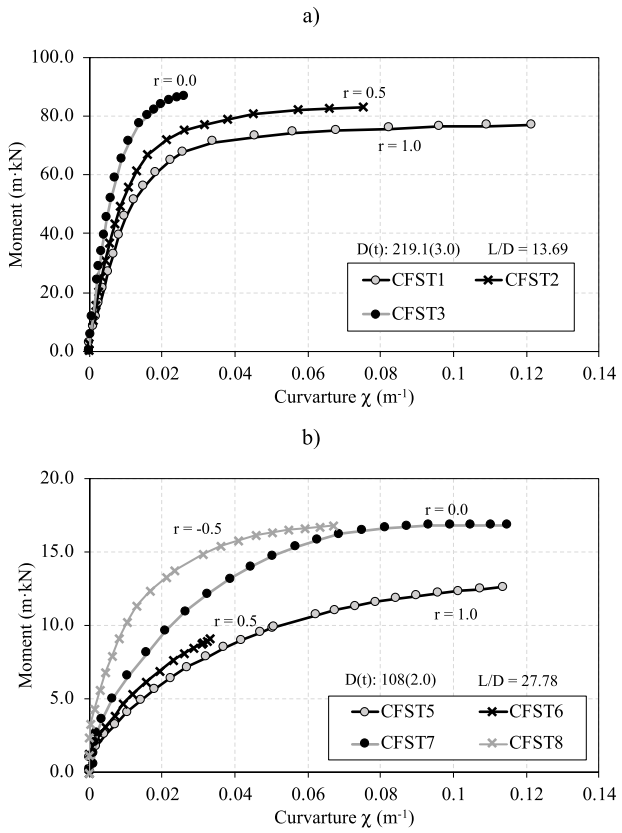

Fig. 10. Measured moment – curvature line (M- χ) in section A-A (L/2). a) CFST1-CFST3. b) CFST5-CFST8.

Table 3
Comparison of equations for second order analysis.

Eurocode 4	AISC 360–16
$M_{tot} = k \cdot N_{Ed} \cdot e^{top} + k_2 \cdot N \cdot e_0$	$M_{tot} = B_1 \cdot (P_r \cdot e^{top})$
$k = \frac{\beta}{1 - \frac{N_{Ed}}{N_{cr,eff}}}$	$B_1 = \frac{C_m}{1 - \frac{P_r}{P_{e1}}}$
$k_2 = \frac{1}{1 - \frac{N_{Ed}}{N_{cr,eff}}}$	
$\beta = 0.66 + 0.44 \cdot \frac{e^{top}}{e^{bot}} \geq 0.44$	$C_m = 0.6 + 0.4 \cdot \frac{e^{top}}{e^{bot}}$
$N_{cr,eff} = \frac{\pi^2 \cdot EI_{eff,II}}{L^2}$	$P_{e1} = \frac{\pi^2 \cdot EI^*}{L^2}$
$EI_{eff,II} = 0.9 \cdot (E_a \cdot I_a + 0.5 \cdot E_{cm} \hat{A} \cdot I_c)$	$EI^* = 0.64 \cdot (E_s \cdot I_s + C_3 \cdot E_c \cdot I_c)$
$e_0 = \frac{L}{300}$	$C_3 = 0.45 + 3\left(\frac{A_s}{A_g}\right) \leq 0.9$
$E_{cm} = 22.000 \cdot \left(\frac{f_c}{10}\right)^{0.3}$ (MPa)	$E_c = 0.043 \cdot w_c^{1.5} \cdot \sqrt{f_c}$ (MPa)
	w_c: weigth of concrete in S.I

constant bending moment by using an equivalent moment factor to convert the problem into the equivalent one under constant bending moment. This factor is called β in the Eurocode 4 [7] and C_m in AISC 360–16 [12]. In both cases, the equivalent moment factor works as a reduction factor (value lower than 1.0) which depends on the loading eccentricity ratio (r). A summary of the equations to take into account the second order effects for both standards are listed in Table 3.

In turn, the deflection measurements carried out during the experiments by the LVDTs at maximum axial load ($\Delta_{N_{max}}$) allowed for the assessment of the total bending moment, including the second order effects, simply using the following expression:

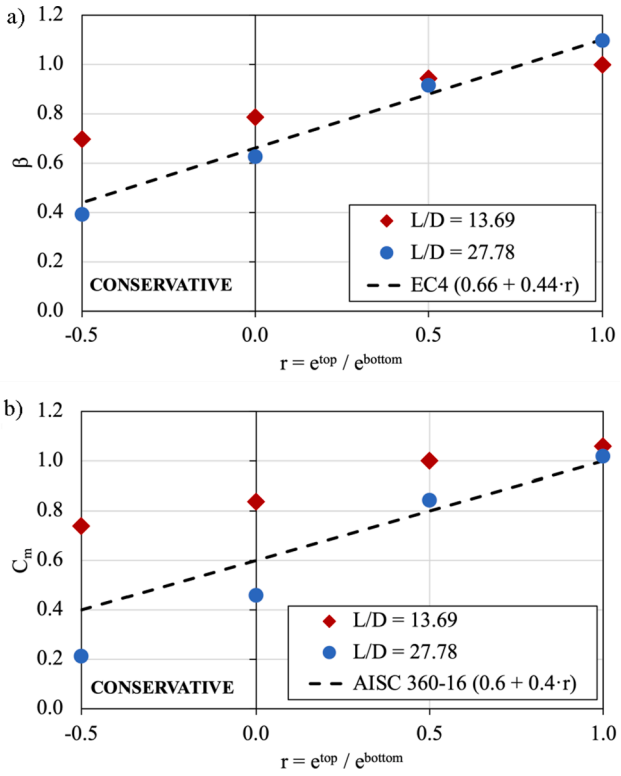

Fig. 11. Equivalent moment factor (β-C_m). Measured and predicted. a) EC4. b) AISC 360–16.

$$M_{tot} = N_{exp} \cdot (e^{top} + \Delta_{N_{max}}) \quad (5)$$

Therefore, the experimental calculation of the total bending moment from Eq. (5) can be directly compared against the equations provided by the standards (Table 3) in order to obtain an experimental value of the equivalent moment factor, β or C_m. The results from this computation are listed in Table 2 as β_{exp} or $C_{m,exp}$ and also plotted in Fig. 11 where the values proposed by the standards are displayed as a dashed black line.

As it was explained before, the equivalent moment factor may be understood as a reduction factor to transform the less critical non-constant bending moment problem to a more critical one under constant bending to facilitate the design process. Points for β or C_m over the dashed black line (see Fig. 11) reveal higher experimental values than predictions provided by standards. Additionally, it should be noted that Fig. 11 shows in blue dots predicted β or C_m values for slenderer columns (L/D = 27.78, CFST5 to CFST8) but in red diamonds for less slender ones (L/D = 13.69, CFST1 to CFST 4).

The direct Fig. 11 observation reveals the following important findings:

- The Eurocode 4 framework for the second order effects assessment of these beam-columns shows more accurate results than AISC 360–16 in terms of the equivalent moment factor.
- The expressions provided by Eurocode 4 and AISC 360–16 for the equivalent moment factor, β or C_m respectively, show conservative predictions for beam-columns with length-diameter ratio equal to 27.78 but unconservative predictions for beam-columns with lower length-diameter ratio (L/D = 13.69). Additionally, the discrepancy of these unconservative predictions increases for lower loading eccentricity ratio (r).

The second finding described above may indicate that the equivalent moment factor not only depends on the loading eccentricity ratio (r) but also on the column slenderness as it was proposed by other authors for

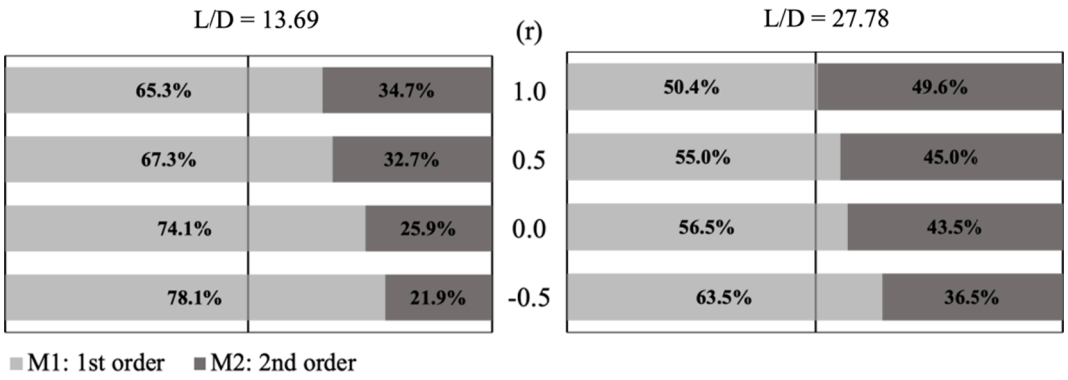

Fig. 12. First and second order bending moment obtained from experiments.

reinforced concrete columns [18]. Additionally, this fact may explain the Eurocode 4 unsafe predictions found by *Zeghiche and Chaoui* [6] and already noted in the introduction of this paper. Indeed, the specimens tested by *Zeghiche and Chaoui* [6] presented double curvature and a length-diameter ratio of 12.5.

In turn, Fig. 12 shows the comparison between the first and second order bending moments for all tested specimens. This figure reveals that the second order effects are less important for double curvature ($r < 0$) and also, in general, for lower length-diameter ratio (L/D).

Finally, it should be noted that the assessment of the equivalent moment factor was done assuming the value for the column stiffness provided by the standards as accurate enough. However, this fact is also controversial. Indeed, both values, the equivalent moment factor and the column stiffness for the second order analysis are connected and should be deeply studied in future research.

5. Conclusions

This paper presents the test results of eight circular concrete-filled steel tubular beam-columns, 3 m long, subjected to unequal load eccentricities in both column ends. This experimental program extends the number of experiments available on this loading typology for CFST columns, which are nowadays limited. The main conclusions obtained through the analysis of the test results are listed hereafter:

- The application of unequal load eccentricities in CFST beam-columns provides an increase on the maximum resisting load but a decrease on the column ductility. This finding was observed for columns with a length-diameter ratio (L/D) of 27.78 but was not evident for columns with lower length-diameter ratio (L/D = 13.69).
- Eurocode 4 and AISC 360–16 provisions for the equivalent moment factor, β or C_m respectively, were assessed using the test results. This assessment concluded that Eurocode 4 proposal present a more accurate prediction. Additionally, unconservative predictions were observed for CFST beam-columns under double curvature loading, which presents a slenderness ratio equal to 13.69. On the contrary, conservative predictions were obtained in both cases for beam-columns with higher length-diameter ratio (L/D = 27.78).
- It was found that the current provisions for the equivalent moment factor from Eurocode 4 and AISC 360–16 depending only on the loading eccentricity ratio (r) do not capture the influence of other parameters like the column slenderness, which revealed to be evident from the test results observation done in this paper. Therefore, further research should be done to introduce other parameters in order to improve the accuracy of the current equations.

CRediT authorship contribution statement

V. Albero: Investigation, Writing – original draft. **C. Ibañez:** Investigation, Formal analysis, Writing – original draft. **D. Hernández-Figueirido:** Investigation, Methodology, Writing – review & editing. **A. Piquer:** Investigation, Writing – review & editing, Project administration.

Declaration of Competing Interest

The authors declare that they have no known competing financial interests or personal relationships that could have appeared to influence the work reported in this paper.

Acknowledgements

The authors would like to express their sincere gratitude to Universitat Jaume I for the funding provided through the project UJI-B2018-58. Funding for open access charge: CRUE-Universitat Jaume I.

References

[1] Zhao X-L, Han L-H, Lu H. Concrete-filled tubular members and connections. CRC Press; 2010.
[2] Han L-H, Li W, Bjorhovde R. Developments and advanced applications of concrete-filled steel tubular (CFST) structures: Members. J Constr Steel Res 2014;100:211–28. https://doi.org/10.1016/j.jcsr.2014.04.016.
[3] Goode D, Lam D. Concrete-filled steel tube columns-tests compared with Eurocode 4. Compos Constr Steel Concr VI 2011:317–25. https://doi.org/10.1061/41142(396)26.
[4] Leon R, Perea T, Hajjar J, Denavit M. Concrete-filled tubes columns and beam-columns: a database for the AISC 2005 and 2010 specifications, 2011, p. 203–12.
[5] Kilpatrick AE, Rangan BV. Tests on high-strength concrete-filled steel tubular columns. ACI Struct J 1999;96. https://doi.org/10.14359/618.
[6] Zeghiche J, Chaoui K. An experimental behaviour of concrete-filled steel tubular columns. J Constr Steel Res 2005;61:53–66. https://doi.org/10.1016/j.jcsr.2004.06.006.
[7] CEN. EN 1994-1-1. Eurocode 4: Design of composite steel and concrete structures. Part 1-1: General rules and rules for buildings; 2004.
[8] Wang YC. Tests on slender composite columns. J Constr Steel Res 1999;49(1):25–41. https://doi.org/10.1016/S0143-974X(98)00202-8.
[9] BSI British Standards Institution. BS 5400-5:2005 Steel concrete and composite bridges. Code of practice for design of composite bridges; 2005.
[10] Hernández-Figueirido D, Romero ML, Bonet JL, Montalvá JM. Influence of slenderness on high-strength rectangular concrete-filled tubular columns with axial load and nonconstant bending moment. J Struct Eng 2012;138(12):1436–45. https://doi.org/10.1061/(ASCE)ST.1943-541X.0000590.
[11] Hernández-Figueirido D, Romero ML, Bonet JL, Montalvá JM. Ultimate capacity of rectangular concrete-filled steel tubular columns under unequal load eccentricities. J Constr Steel Res 2012;68:107–17. https://doi.org/10.1016/j.jcsr.2011.07.014.
[12] American Institute of Steel Construction. ANSI/AISC 360-16 Specifications for Structural Steel Buildings; 2016.

[13] Jin L, Fan L, Du X. Meso-scale modeling of size effect in eccentrically-loaded squared CFST columns: Influence of eccentricity and confinement effect. Thin-Walled Struct 2021;169:108455. https://doi.org/10.1016/j.tws.2021.108455.
[14] Lin S, Zhao Y-G, Lu Z-H. Fibre beam element models for nonlinear analysis of concentrically loaded circular CFT columns considering the size effect. Eng Struct 2020;210:110400. https://doi.org/10.1016/j.engstruct.2020.110400.
[15] Espinós A, Albero V, Romero ML, Mund M, Meyer P, Schaumann P. Non-constant biaxial bending capacity assessment of CFST columns through interaction diagrams. Steel Compos Struct 2019;32. https://doi.org/10./scs.2019.32.4.521.
[16] Patel VI, Liang QQ, Hadi MNS. Nonlinear analysis of circular high strength concrete-filled stainless steel tubular slender beam-columns. Eng Struct 2017;130:1–13. https://doi.org/10.1016/J.ENGSTRUCT.2016.10.004.
[17] Han L-H, Zhao X-L, Tao Z. Tests and mechanics model for concrete-filled SHS stub columns, columns and beam-columns. Steel Compos Struct 2001;1:51–74. https://doi.org/10.12989/scs.2001.1.1.051.
[18] Rangan PKS, BV. Reinforced concrete columns under unequal load eccentricities. ACI Struct J n.d.;100. https://doi.org/10.14359/12661.